Nanobelt and nanosaw structures of II-VI semiconductors

Christopher Ma, Daniel Moore, Yong Ding, Jing Li and Zhong Lin Wang*

School of Materials Science and Engineering,
Georgia Institute of Technology, Atlanta, GA 30332-0245, USA
E-mail: zhong.wang@mse.gatech.edu
***Corresponding author

Abstract: The II-VI semiconductors are important optoelectronic, luminescent, and lasing materials. This paper presents a review on synthesis, structure, and growth mechanisms of one-dimensional nanostructures of ZnS, CdSe, ZnSe, CdS and CdO. The two most frequently received wurtzite structures of these materials are 'nanobelts' and 'nanosaws'. The nanosaws are suggested to be a result of atomic-termination induced asymmetric growth due to the cation-terminated, catalytically active (0001) surface, while the anion-terminated (000$\bar{1}$) is chemically inactive. It has also been shown that the phase transformation from wurtzite to zinc blend could also be a factor in initiating the growth of the saw teeth. The applications and nanodevices that have been built using nanobelts are also presented.

Keywords: nanobelt; nanosaw; II–VI Semiconductors; CdSe; CdS; ZnS; ZnSe; nanoribbon.

Biographical notes: Christopher Ma is a PhD candidate in Materials Science and Engineering at the Georgia Institute of Technology. He graduated in 2000 from Coe College with a BA in Physics. He is a Molecular Design Institute (MDI) Fellow (2001–2002) and a Presidential Fellow. Currently, his research interests are synthesis and characterisation of one-dimensional II-VI semiconductors.

Daniel Moore is a PhD candidate in Materials Science and Engineering at the Georgia Institute of Technology. He graduated in 2001 from the University of Chicago with an AB in Physics and Mathematics. He is a MDI Fellow (2002–2003), a Presidential Fellow, and a Nanoscience and Nanotechnology Fellow (2003–2004). Currently, his research interests are one-dimensional non-oxide nanostructures and nanoscale materials for biomedical applications.

Yong Ding received his PhD degree in condensed matter physics from Nanjing University in 2001. He was a research scientist in Institut fuer Festkoerperforschung, Forschungszentrum Juelich GmbH, Germany during 2002-2003. He is now a Postdoctoral Fellow at Georgia Institute of Technology. His research interests are focused on the synthesis, charaterisation and application of low-dimensional materials.

Dr. Jing Li received her PhD in Materials Sciences and Engineering from Berlin University of Technology, Germany in 1994. She now is a Postdoctoral Fellow in the School of Materials Science and Engineering, Georgia Institute of Technology. Dr. Li's research focuses on the property-structure relationship in the fields of nanomaterials and other advanced materials using high-resolution transmission electron microscopy.

Dr. Zhong Lin Wang is Regents' Professor and Director, of the Center for Nanoscience and Nanotechnology, Georgia Institute of Technology. He has authored and co-authored four scientific reference and textbooks, over 350 journal papers, and 40 review papers and book chapters, and has edited and co-edited ten volumes of books on nanotechnology, and held eight patents and provisional patents. Dr. Wang is one of the World's top 25 most cited authors in nanotechnology from 1992–2002. He discovered the nanobalance in 1999, the nanobelts in 2001, and the single-crystal nanorings in 2004. The paper on nanobelt was the second most cited paper in chemistry in 2001–2003 (*ISI, Science Watch*). He was elected to the European Academy of Science in 2002, received the 2001 S.T. Li prize for Outstanding Contribution in Nanoscience and Nanotechnology, the 2000 Georgia Tech Faculty Research Award, the 1999 Burton Medal from Microscopy Society of America, 1998 US NSF CAREER award, and 1998 China-NSF Oversea Outstanding Young Scientists Award. He is a member of the editorial board of over ten journals. His most recent research focuses on oxide nanobelts and nanowires, in-situ techniques for nano-scale measurements, self-assembly nanostructures, fabrication of nano devices for biosensing, and properties of magnetic nanostructures. http://www.nanoscience.gatech.edu/zlwang/

1   Introduction

Nanoscience and technology is a new and dominant player in the scientific arena. Still in its infancy, the basic scientific concepts that govern this field are not fully understood and are continually being explored. The first aspect of nanoscience to gain notoriety was the novel properties of quantum dots. These zero-dimensional structures displayed phenomena that had previously never before been seen in the bulk. Cadmium Selenide quantum dots, the most intensively studied quantum dot material, demonstrates a strong size dependence on their physical properties [1–3]. Brus [4] and then later his coworkers Alivisatos et al. [5], Murray et al. [6] and Bawendi et al. [7] were some of the first scientists to correlate the quantum confinement of these zero-dimension CdSe nanostructures to an induced higher energy shift with decreasing size. This led to a flood of research investigating the size dependence of the luminescent properties of quantum dots [8–11]. Yet despite their luminescence, interest in quantum dots has waned in recent years due to their limited applications in some special areas.

In the early 1990's, Iijima [12] burst onto the scene with the discovery of a one-dimensional (1D) nanostructure, the carbon nanotube. Carbon nanotubes display interesting electronic and mechanical properties, such as ballistic conduction [13] and high tensile and elastic moduli [14]. This sparked an entirely new avenue of research in the nanoscience and technology community. Now nanorods [15–17], nanowires [18–21], nanotubes [22–24], and nanobelts [25–29] of varying materials have been successfully synthesised. And unlike its predecessor, 1D nanostructures demonstrate novel luminescent [30,31], electronic [13,32], and mechanical properties [33,34].

Possible applications for these structures range from waveguides [30] to gas/biological sensors [35], nanotweezers [36] to microcavity lasers [37].

By taking the advantages offered both by the CdSe quantum dots and the 1D nanostructures, developing of II-VI based semiconductor 1D nanostructures is of great interest. ZnO is probably the most typical II-VI semiconductor, which exhibits a wide range of nanostructures. We have systematically reviewed the nanostructures formed by ZnO [38]. This paper reviews the nanobelts and nanosaw structures that have been synthesised for the II-VI semiconductors other than ZnO. Specific properties can be tailored to the nanobelts by controlling growth direction and the surface facets, which may make these structures one of the most important discoveries in the field of 1D nanomaterials. The growth mechanisms of the nanostructures will be discussed, and some potential applications will be illustrated.
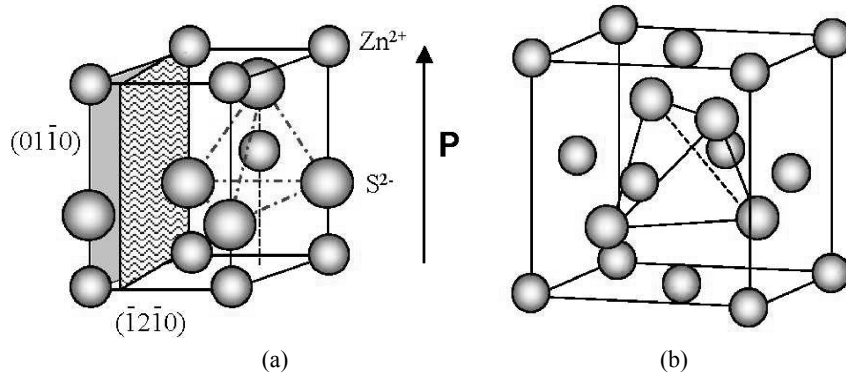
2   Crystal structures

A common characteristic all II-VI semiconductors share is a propensity to form into the wurtzite crystal structure given the right conditions. We now use ZnS as an example to illustrate the structural characteristics of wurtzite. Wurtzite has a hexagonal unit cell (space group *P6₃mc*). The structure of ZnS, for example, can be simply described as a number of alternating planes composed of tetrahedrally coordinated S^{2-} and Zn^{2+} ions, stacked alternatively along the *c*-axis (Figure 1(a)). The tetrahedral coordination in ZnS results in non-central symmetric structure and piezoelectricity. Another important characteristic of ZnS is the polar surfaces. The most common polar surface is the basal plane. The oppositely charged ions produce positively charged Zn-(0001) and negatively charged S-(000$\bar{1}$) polar surfaces, resulting in a normal dipole moment and spontaneous polarisation along the *c*-axis as well as a divergence in surface energy. Structurally, ZnS has three-types of fast growth directions: <2$\bar{1}$$\bar{1}$0> (±[2$\bar{1}$$\bar{1}$0], ±[$\bar{1}2\bar{1}$0], ±[$\bar{1}$$\bar{1}$20]); <01$\bar{1}$0> (±[01$\bar{1}$0], ±[10$\bar{1}$0], ±[1$\bar{1}$00]); and ±[0001]. Together with the polar surfaces due to atomic termination, ZnS exhibits a wide range of novel structures by tuning the growth rates along these directions.

Wurtzite is the most stable structure for CdS and CdSe and the other II-VI semiconductors have previously been observed to exhibit the wurtzite crystal structure [39–41]. This is an important characteristic for these materials, because the intrinsic asymmetric nature of wurtzite in ioniclly bonded materials gives rise to a piezoelectric phenomenon. This piezoelectric property in nanobelts lends them to applications such as nanocantilevers [42] in scanning probe microscopy (SPM). The use of nanobelt cantilevers will increase the sensitivity ~35–1800 times that of conventional cantilevers. The nanocantilevers could be used in mass, biological, force, thermal, pressure, and chemical sensors [43–45]. Through the successful synthesis of II-VI semiconductors in a nanobelt form, a wide range of mechanical and optoelectronic application may be possible for these materials, which is why the continued study of II-VI semiconductors is of the greatest importance.

Zinc blend is the second common structure for the II-VI compound semiconductor (Figure 1(b)). Bulk ZnS, for example, is the most typical example of the structure. Zinc blend has a cubic unit cell and it is made of two interpenetrating face centered cubic (FCC) sublattices of Zn and S with a displacement of 1/4[111] along the diagonal direction.
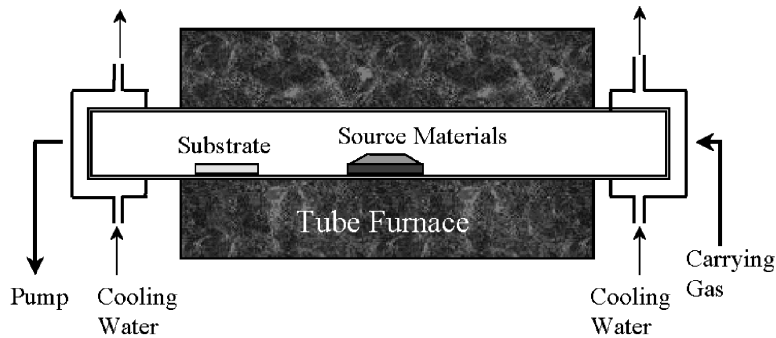
Figure 1   (a) The wurtzite ZnS structure and (b) the zinc blend structure for the II-VI
            semiconductors

$(01\bar{1}0)$

Zn^{2+}

P

S^{2-}

$(\bar{1}2\bar{1}0)$

(a)   (b)

3   Synthesis technique

The nanostructures to be reviewed in this paper were synthesised by a thermal
evaporation process. In principle, the thermal evaporation technique is a simple process
in which condensed or powder source material(s) is vaporised at elevating temperature
and then the resultant vapour phase(s) condenses under certain conditions (temperature,
pressure, atmosphere, substrate, etc.) to form the desired product(s). The processes are
usually carried out in a horizontal tube furnace, as shown in Figure 2, which is composed
of a horizontal tube furnace, an alumina tube, a rotary pump system and a gas supply and
control system. A view window is set up at the left end of the alumina tube, which is used
to monitor the growth process. The right-hand end of the alumina tube is connected to the
rotary pump. Both ends are sealed by rubber O-rings. The ultimate vacuum for this
configuration is $\sim 2 \times 10^{-3}$ Torr. The carrying gas comes in from the left end of the
alumina tube and is pumped out at the right end. The source material(s) is loaded on an
alumina boat and positioned at the center of the alumina tube, where the temperature is
the highest. Alumina substrates were placed downstream for collecting growth products.
This simple set up can achieve high control on the final product.

Figure 2   Experimental setup for the thermal evapouration process of synthesising nanobelts.
            The source material is placed in the center of the horizontal tube furnace and target
            substrates are placed in a lower temperature zone, 'downstream' from the source.
            This setup can be used to achieve a high level of control over the final product

There are several processing parameters such as temperature, pressure, carrier gas (including gas species and its flow rate), substrate and evapouration time period, which can be controlled and need to be selected properly before and/or during the thermal vapourisation [46]. The source temperature selection mainly depends on volatility of the source material(s). Usually, it is slightly lower than the melting point of the source material. The pressure is determined according to the evapouration rate or vapour pressure of the source material(s). The substrate temperature usually drops as the distance of its location being away from the position of the source material(s). *The local temperature determines the type of product to be received.* It is also noted that the thermal evapouration process is very sensitive to the concentration of oxygen in the growth system. Oxygen influences not only the volatility of the source material(s), the stoichiometry of the vapour phase, but also the formation of the product(s). In the present study, after evacuating the alumina tube to $\sim 2 \times 10^{-3}$ Torr, thermal vapourisation was conducted following a designed heating rate and holding duration at a pressure of 200–600 Torr and a carrier gas of 50 sccm (standard cubic centimeters per minute). The on and off time as well as the length of inletting the carrier gas could greatly affect the growth kinetics.
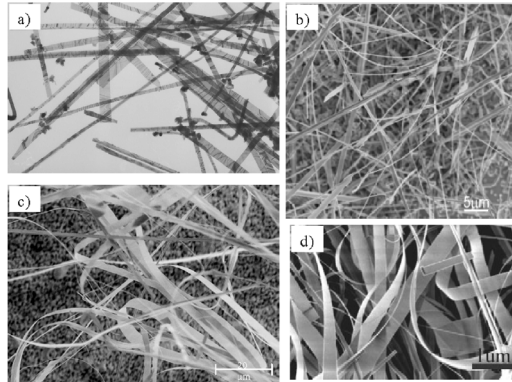
The as-deposited products were characterised and analysed by X-ray diffraction (XRD) (Philips PW 1800 with Cu Kα radiation), scanning electron microscopy (SEM) (LEO 1530 FEG), transmission electron microscopy (TEM) (Hitachi HF-2000 FEG at 200 kV and JEOL 4000EX high resolution TEM (HRTEM) at 400 kV), and energy dispersive x-ray spectroscopy (EDS).

4   Novel nanostructures
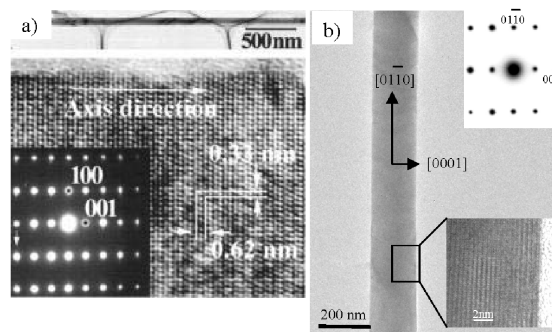
4.1   ZnS nanobelts

The first of the II-VI semiconductors to be grown as a nanobelts was ZnS. Several groups have reported the successful synthesis of ZnS nanobelts using a simple thermal evapouration technique [47–52]. Thermal evapouration is the most common synthesis method for growing any material in a belt-like nanostructure. Figure 3 gives TEM and SEM images of four different research groups using slight variation of the parameters in the thermal evapouration process of ZnS. It can easily be seen from this figure that all of the morphologies are similar to one another. Typically, the ZnS nanobelts have the wurtzite crystal structure at elevated temperatures. A metastable phase, wurtzite ZnS nanobelts can be left for several months without any phase transformation to the zinc blend form. However, Ma et al. [47] have shown that by bombarding a ZnS wurtzite nanobelt with a 200 kV electron beam, it is possible to locally induce the phase change from metastable wurtzite to the more stable zinc blend structure.

Figure 3   (a) TEM (from [52], with permission) and (b, c, d) SEM images (from [47,48,51], respectively, with permissions) of ZnS nanobelts and nanowires, showing how variance in the synthesis parameters greatly affects the product received

Thermodynamically, the fastest growth direction for a wurtzite structure is the [0001] (see Figure 4(a)). However by altering the synthesis conditions, growth rates of slower crystalline planes can be increased. It is common to observe ZnS nanobelts with [0001] and [01$\bar{1}$0] growth directions within the same synthesis run. Li et al. [52] synthesised ZnS nanobelts with growth directions of [01$\bar{1}$0] (see Figure 4(b)), suppressing the [0001] growth direction in certain nanobelts. Altering the growth direction can have enormous repercussions in morphology and physical properties of the nanobelts. Moore et al. [53] grew belts along the [01$\bar{1}$0], making the side facets of the nanobelts the positively charged (0001)-Zn and negatively charged ($000\bar{1}$)-S.
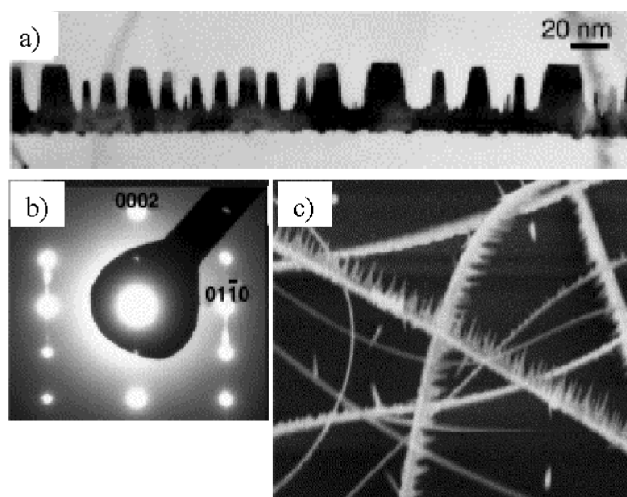
Figure 4   TEM images and corresponding electron diffraction patterns from ZnS nanobelts showing that the common growth directions are [0001] (from [49], with permission) and [01$\bar{1}$0] (from [52], with permission)

4.2   *ZnS nanosaws*

Another interesting growth morphology is the formation of nanosaw structure, which is the result of preferred growth on one side of the nanobelt. Figures 5(a) and (c) are typical TEM and SEM images, respectively, of the ZnS nanosaws, with saw teeth along [0001], saw direction [01$\bar{1}$0] and the saw ribbon defined by (2$\bar{1}\bar{1}$0). This asymmetric growth behavior is similar to that of ZnO, and is the result of surface termination induced growth.

Figure 5 Typical (a) TEM, (b) diffraction pattern and (c) SEM image of ZnS nanosaws. The diffraction pattern in (b) shows that the growth direction is [01$\bar{1}$0] and that the side surfaces are the polar (0001) surfaces (from [53], with permission)

4.3 CdSe Nanobelts

CdSe is of particular importance because of its well documented quantum confinement effects [1–11]. One of the first type of 1D nanostructure to be made from this material were nanorods [15,54–56]. Shape controlled synthesis of CdSe nanorods [57,58] and template-assisted synthesis of CdSe nanowires [59,60] and nanotubes [61] have been demonstrated through electrochemical and chemical approaches. Two-dimensional arrays of CdSe pillars have also been fabricated using e-beam lithography [62]. However these nanowires and nanotubes are composed of nanosize grains, which are polycrystalline in nature. The grain boundary scattering could greatly affect the optoelectronic performance and a single crystal alternative would seem ideal. Ma et al. [63] were able to synthesise nanobelts that were single crystal and defect-free through a thermal evapouration of commercial grade (99.995% purity) CdSe powder. Figure 6 gives typical SEM images of the belt and saw-like CdSe nanostructure. By controlling the growth conditions, the morphology can be changed from a belt-like structure to a saw-like structure, which is governed by the spontaneous polarisation-induced asymmetric (SPA) growth mechanism. Both the belt and saw-like structures grow along the [01$\bar{1}$0] and have top and bottom surfaces of $\pm$(2$\bar{1}$$\bar{1}$0). The growth of the saw structure is a two-step process: first (see Figure 7(c)) a belt is formed via the VLS mechanism as the CdSe is guided by a Au catalyst along the, [01$\bar{1}$0] or [01$\bar{1}$1] growth direction (see Figures 7(a) and (e)); the second step is the growth of the 'teeth' of the nanosaws along the [0001]. Through an intensive study of these CdSe nanosaws, Ding et al. [64] suggest that the growth of the teeth can be attributed to factors: self-catalysed effects of the more chemically active Cd-terminated (0001) surface and a secondary epitaxial nucleation process owing to the zinc-blend to wurtzite phase transformation.

Figure 6   Typical SEM images of CdSe nanosaws, with teeth along the [0001] directions
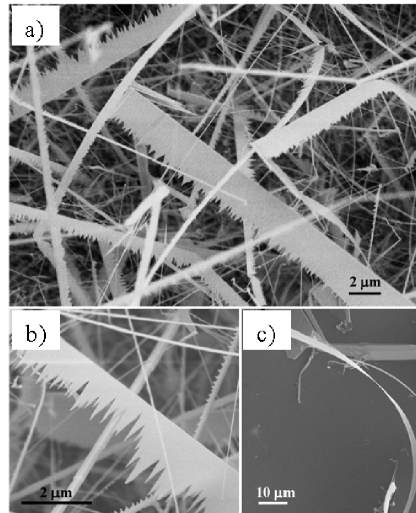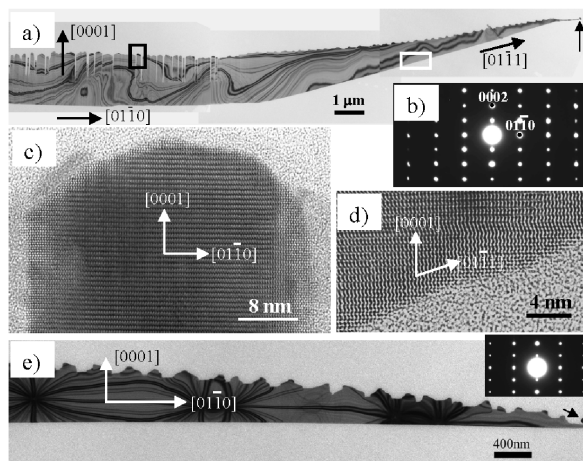   (from [63], with permission)

Figure 7   (a) TEM image of a CdSe nanosaw, (b) the corresponding electron diffraction pattern,
           showing the ribbon direction is [01$\bar{1}$0] and switches to [01$\bar{1}$1], while the teeth
           direction is [0001]. (c,d) High-resolution TEM images recorded from the areas
           indicated by black and white boxes in (a), respectively. The nanosaw has a high
           crystallinity and is free from dislocations, although stacking fault parallel to (0001) can
           be found occasionally and (e) TEM image of a CdSe nanosaw and the corresponding
           electron diffraction pattern (from [63], with permission)
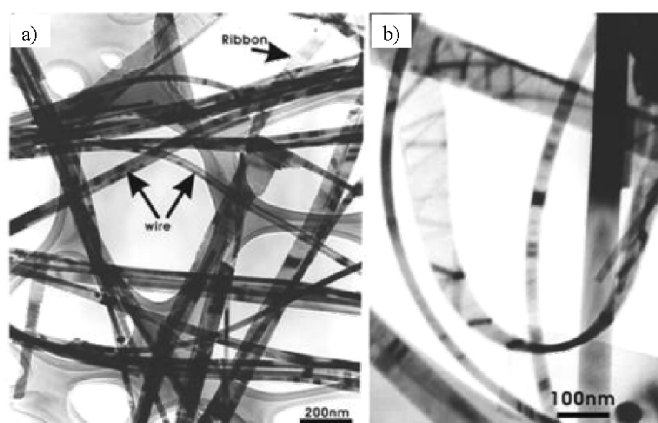

4.4   CdSe nanosaws

Spontaneous Polarization-induced Asymmetric (SPA) growth is a phenomenon uniquely
observed in wurtzite nanobelts. The belt-like structure allows for faceted growth that,
because of the difference levels of chemical activity between the two polarised surfaces,
produces preferred growth on one (typically the cation terminated) of the polar surfaces.

SPA growth has been observed in ZnO [65], ZnS [53], and CdSe [63]. Figure 5 shows SEM images of CdSe nanoribbons that have nanosaw structure. The saw teeth are at one side and the other side is straight and smooth.

4.5   ZnSe nanobelts

ZnSe, like ZnS, has a cubic crystal structure in its most stable state. However as seen with ZnS, the II-VI semiconductors can form the wurtzite crystal structures given the correct synthesis technique and conditions. Jiang et al. [41] deviated from the typical synthesis route of thermal evapouration and employed a laser ablation technique. The principle behind both synthesis procedures is the same, sublimate a starting material and carry the vapour to cooler regions for deposition. Laser ablation, however, has the benefit of increasing the temperature of the source at such a rapid rate that the stoichometery of the starting material is maintained in the vapour. This allows for more complex starting materials to be used (like ternary compounds), since there is no dissociation or chemical reaction of vapour as it is transported from the source to the deposition zones. In particular Jiang et al. used a KrF pulsed excimer laser and a horizontal tube furnace with a quartz tube mounted inside. High purity (>99.9%) ZnSe powder was pressed and used as a target. Silicon wafers were coated with a 30 Å gold film, which acted a catalyst for growth, and were placed 30 cm downstream of the target. The results from their experiment revealed a combination of nanowires and nanobelts within the deposited material. The ratio of nanowires to nanobelts was 60–40% in favour of the nanowires. Through an examination of the as-synthesised material, the microscopy revealed that ZnSe nanowires formed via the well-known vapour–liquid–solid (VLS) mechanism, while the ZnSe nanobelts formed through the vapour-solid (VS) mechanism. The synthesised ZnSe have uniform cross sections throughout and thickness to width ratios for the ZnSe nanobelts are around 1:10. Like other nanobelts, the ZnSe belts demonstrate high flexibility without fracture (Figure 8), which is not observed in bulk ceramic materials.
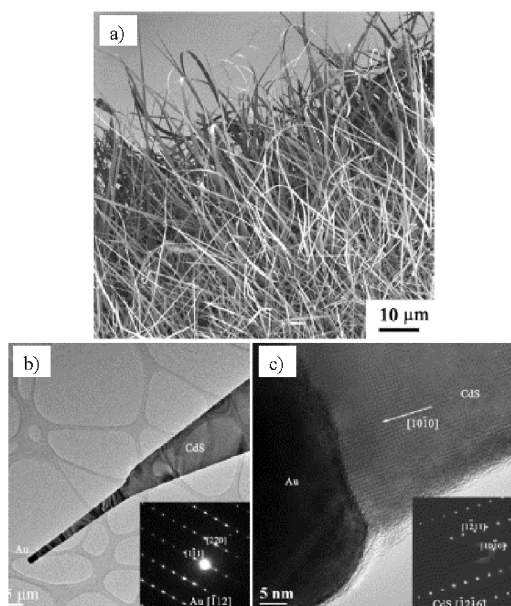
Figure 8   (a) ZnSe nanobelts and nanowires are grown in the same process and temperature region and (b) The bending of the ZnSe belts reveals the high flexibility without fracture of the structure (from Jiang et al. [41], with permission)

4.6   *CdS nanobelts*

Catalytic growth was used to synthesise CdS nanobelts [66], although it should be noted that use of a catalyst is not necessary to grow CdS nanobelts [67]. Dong et al. used a thermal evapouration process whereby the CdS vapour would preferentially nucleate on Au covered Tungsten foils that had been placed within the deposition region (see Figure 9(a)). The results were wurtzite CdS nanobelts growing along [10$\bar{1}$0]. An apparent consequence of using a catalyst is non-uniform cross sections in the belts. When growth initially occurs, the size of the nanobelt is restricted to the size of the Au catalyst, which is illustrated in Figure 9(b). Dong et al. suggest that after the initial growth of the nanobelt, CdS gas directly deposit onto the belt via the VS mechanism, causing it to grow larger in width. A more intensive study must be done before definitive conclusion can be drawn to the exact mechanism that accounts for the non-uniform cross section of these catalytically grown CdS nanobelts.
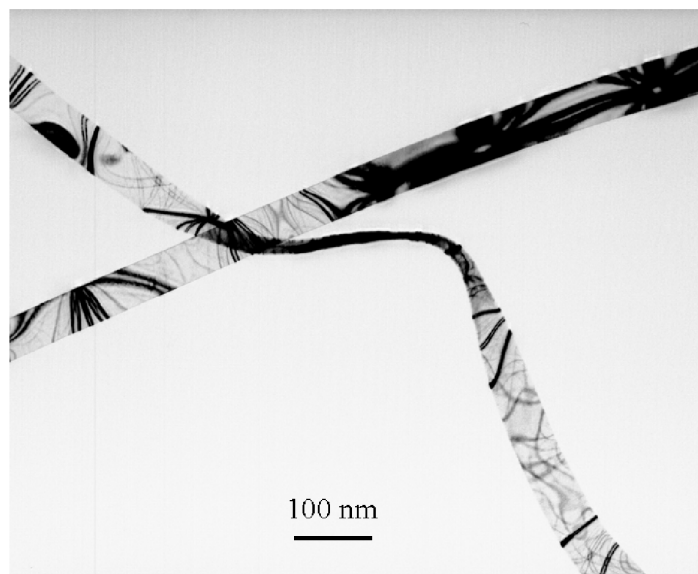
Figure 9   (a) The CdS nanobelts preferentially grow on the Au covered Tungsten foils, (b,c) TEM images of the CdS nanobelts showing that they are wurtzite and growth with the catalyst is along the [10$\bar{1}$0] direction (from Dong et al. [66], with permission)

4.7   *CdO nanobelts*

Nanobelts of CdO with NaCl cubic structure were also synthesised by evapourating CdO powders (purity: 99.998%, melting point: 1430°C) at 1000°C [25]. Besides CdO nanobelts, many single crystalline CdO sheets with sizes on the order of several to several tens of micrometers were also formed. These CdO sheets usually have shapes in rectangle, triangle, and parallelogram. The lengths of the CdO nanobelts are usually less than 100 μm, and their widths are typically 100–500 nm (Figure 10). Electron diffraction pattern shows that the nanobelts grow along [100], and their surfaces are enclosed by $\pm$(001) and $\pm$(010) facets.

Figure 10 TEM Image of CdO nanobelt. The widths of the nanobelts are typically 100–500 nm (from [25], with permission)
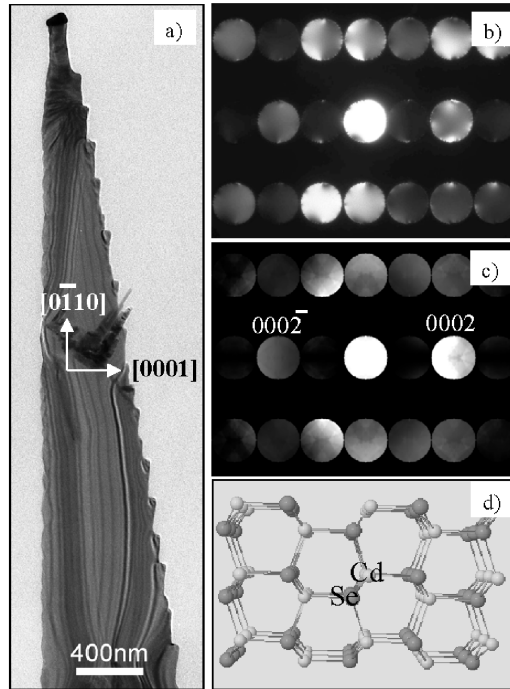

5 Formation of nanosaw structures

5.1 Self-catalysed growth of polar surfaces

The most profound phenomenon of the nanosaw structure is the growth of asymmetric saw teeth on one side and the other side is straight and smooth. From the structure model shown in Figure 1(a), the (0001) surface of wurtzite can terminate with different atom plane. Take CdSe as an example, the (0001) surface is terminated with Cd and the $(000\bar{1})$ is terminated with Se (Figure 11(a)). To quantitatively determine the polarity of the surfaces, convergent beam electron diffraction (CBED) pattern was recorded from the ribbon, as given in Figure 11(b). The intensity distributions in the (0002) and the $(000\bar{2})$ disks are significantly different, which is due to the non-central symmetric structure of CdSe, which can uniquely determine the polarity of the CdSe nanosaws [68]. Quantitative interpretation of the CBED relies on dynamic simulations, which were performed using an improved version of the Bloch wave program [69]. A comparison of the experimental pattern with a theoretically calculated pattern (Figure 11(c)) indicates that the saw teeth grow out of the (0001)-Cd surface. Therefore, the growth of the saw teeth is due to the catalytically active Cd-(0001) surface, while the Se-$(000\bar{1})$ is relatively inactive, producing the asymmetric growth morphology.
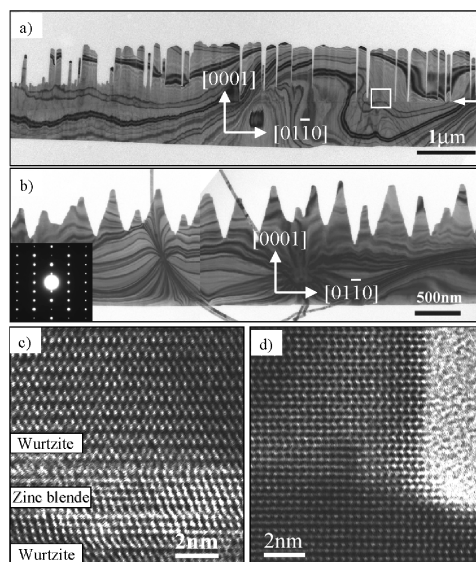
Figure 11 (a) a TEM image of a CdSe nanosaw where the (0001) surface is terminated with Cd
and the (000 $\bar{1}$) surface is terminated with Se, (b) the experimental CBED pattern,
showing the polarity of the different surfaces, is compared, favourably, with the (c)
theoretical CBED pattern and (d) An atomic model of the arrangement of the Cd and Se
atoms in the nanosaw structure

5.2   *Phase transformation*

The most dominant morphology found in samples that exhibit spontaneous
polarization-induced asymmetric (SPA) growth is the 'saw' shape nanobelt, with one side
flat and the other side sharp 'teeth'. Detailed study of CdSe has led to some interesting
discoveries relating to the growth of the saw and teeth structures [65]. As stated
previously, many of the bulk or thin films of II-VI semiconductors can exist in the
typically more stable zinc blende structure, but most of the nanobelts and nanosaws
presented here are dominated by the wurtzite structure (Figures 12(a) and (b)).
High-resolution TEM image recorded near the root of the nanoteeth of CdSe indicates the
existence of a different phase, which is several atomic layers in thickness and
corresponds to the zinc blende structured CdSe (see Figure 12(c)). The zinc blende is a
result of changing the stacking sequence from ABAB for the hexagonally structured
wurtzite to ABCABC. The energies for the two phases are quite close [70] and it is
relatively easy to stimulate phase transformation. Analogous structure has been also
reported for ZnS [47]. The magnitude in morphology oscillation for the saw structure is
much lower than that for the nanoteeth. High-resolution TEM from the saw region found
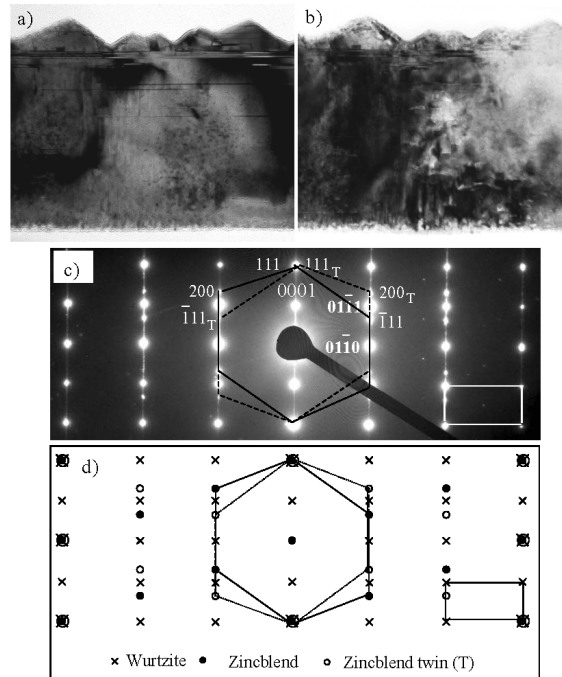neither planar defect nor zinc blend phase.

Figure 12 (a,b) TEM images of the CdSe nanobelts, showing that the belts are dominated by the wurtzite structure rather than the zinc blend structure and (c,d) high resolution TEM images showing the existence of the zinc blend phase near the root of the teeth that is several atomic layers thick

The formation of the one-sided saw structures may be owing to two factors. First, it could be due to the self-catalysed process of the Cd-terminated (0001) surface resulting in the asymmetric growth morphology. Secondly, the growth of the side nanoteeth may also be related to the presence of the zinc-blend layer. From the structural information provided by Figures 12(a) and (c), the top and bottom surfaces of the Wurtzite phase are the $\pm(2\bar{1}\bar{1}0)$ low energy facets, but the corresponding planes for zinc blende phase are $\pm(110)$, which are the high energy facets for cubic system and are thus energetically unfavourable. Therefore, the width of the zinc blende strip is limited for reducing the surface energy, but a continuous growth as driven by the catalytic active Cd-terminated (0001) surface tends to re-nucleate the wurtzite phase. This nucleation is epitaxial but a multiple nuclei case along the length of the nanoribbon is most likely, possibly resulting in the growth of the nanoteeth on one side.

One has to be cautious in identifying phase transformation because electron beam can induce phase transformation as well. Taking ZnS as an example, the wurtzite structured ZnS is unstable under the electron beam illumination in TEM and it may transform to zinc blend structure. Shown in Figures 13(a) and (b) are two images recorded from the same area before and after the sample was illuminated for about 10 minutes under 200 kV electrons, showing an increase in density of planar defects. Electron diffraction pattern recorded from the area shows the co-existence of the hexagonal wurtzite structure and the cubic zinc blend structure (Figures 13(c) and (d)). The orientation relationship between the two phases are: $[2\bar{1}\bar{1}0] \parallel [01\bar{1}]$, and $(0001) \parallel (111)$. The two phases co-exist by sharing the same (0001) or (111) plane. It is also known that the cubic phase ZnS typically has the {111} twins. The existence of the twins is indicated by the electron diffraction pattern, and the diffraction spots and the corresponding indexes from the hexagonal phase, the cubic phase and its twin are illustrated in Figure 13(d).

Figure 13 (a,b) TEM images of a saw-like ZnS nanostructure prior and post illuminated by
the electron beam for ~10 minutes, showing the formation of planar defects,
(c) Electron diffraction pattern recorded from the area, which can be indexed as the
coexistence of the hexagonal and cubic phases with the presence of twins in the cubic
phase and (d) A schematic showing the systematic reflections in corresponding to
the experimental pattern shown in (c), TEM images of a ZnS nanosaw (a) before and
(b) after they were irradiated with a 200 keV electron beam, (c) The diffraction pattern
is post-irradiation and displays the phase transformation from wurtzite to zinc blend that
is induced (from [47], with permission)

6   Applications and nanodevices

For over a decade, II-VI semiconductors have attracted growing interest owing to their
possible application in optoelectronics. The wide band gap II-VI semiconductors are
efficient emitters in the blue to UV spectral range and are likely candidates to replace
materials like GaN in light emitting laser diodes [71]. Despite some similarities, each of
the II-VI semiconductors demonstrate their own unique and novel physical properties.
ZnS has a band gap energy of 3.6 eV [72], displays a high refractive index [73], and a
high transmittance in the visible range [74,75] making this material a strong candidate for
use in optoelectronic devices. However what makes this material so intriguing is its
various luminescent properties. ZnS not only exhibits photoluminescence [76] but also
acousticluminescence [77], triboluminescence [78], electroluminescence [79], and
thermoluminescence [80], lending the material to promising applications in flat panel
display, sensors, and lasers. CdTe and ZnSe have direct band gaps of 1.4 eV [81] and
2.8 eV [82] respectively. CdTe has a high optical absorption coefficient making it ideal
for investigation in solar cells and other photoelectric devices [83], while ZnSe could
potentially be used in short wavelength lasers [84].

The nanostructures of II-VI semiconductors may exhibits some unique properties. Duan et al. [85] have shown that CdS nanowires function as Fabry-Perot optical cavities and used these nanowires as electrically driven lasers. As stated before, CdSe is the most extensively studied quantum nanostructures material due to it strong size-tunable properties, and possible applications for this material include laser diodes [86], nanosensing [9], and biological labeling [87]. Recently Alivisatos et al. demonstrated that CdSe nanorods can have up to 100% polarised luminescence and could be used as nano-emitters or high resolution detectors of polarised light.

Zapien et al. [88] have taken one of the first steps in this direction by studying ZnS nanobelts as room temperature lasers using a photoluminescence technique, whereby a 266 nm laser was used as an excitation source. Figure 14 shows the results of Zapien's study on individual ZnS nanoribbon. Zapien measured the threshold pumping power to be 45 kW/cm^2 (Figure 14(a)) and that it is possible to have an individual ZnS nanobelt to begin lasing at a power density as low as 9 kW/cm^2 (Figure 14(b)). This measured value for threshold pumping is similar to results published earlier using ZnO nanowires as lasers [89]. However, a possible added benefit of using nanobelts is the completely faceted morphology. Nanowires only have facets at the top and bottom surfaces of the wire, whereas nanobelts are made up of six faceted surfaces. The facets can act as reflective mirrors trapping light in the nanostructures.

CdS is an excellent material for optical as well as electronic applications, because of its intrinsically low surface trapping states and, recently, CdS nanobelts been used in device setups. Duan et al. [90] have shown a general approach for using II-VI semiconducting nanobelts as Thin Film Transistor (TFT) channel materials, opening up new opportunities not possible with current poly-Si technologies. Specifically, Duan et al. also have shown CdS nanobelts in conjunction with CdS nanowires as a complementary inverter. The output-input voltage curve from their study is given in Figure 15. The use of nanobelts in this capacity offers a technology platform for high-performance TFTs from high-mobility materials and for novel large-area optoelectronics from II-VI materials.

Figure 14 (a) The threshold pumping power of the ZnS nanobelt is measure to be 45 kW/cm^2 and (b) it is possible to have an individual ZnS nanobelt begin lasing at a power density as low as 9 kW/cm^2 (from [88], with permission)
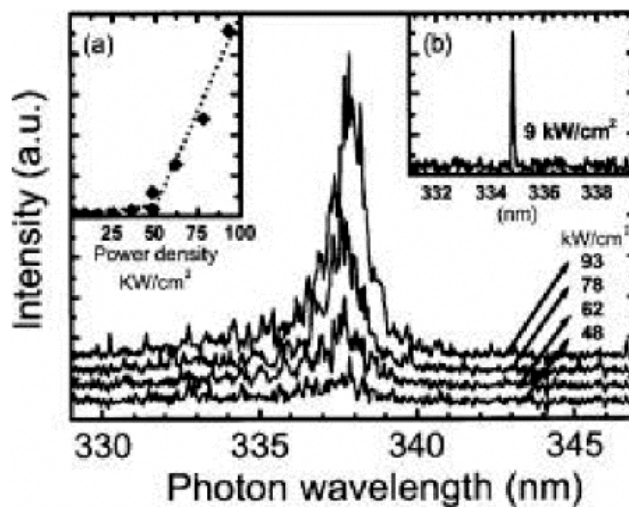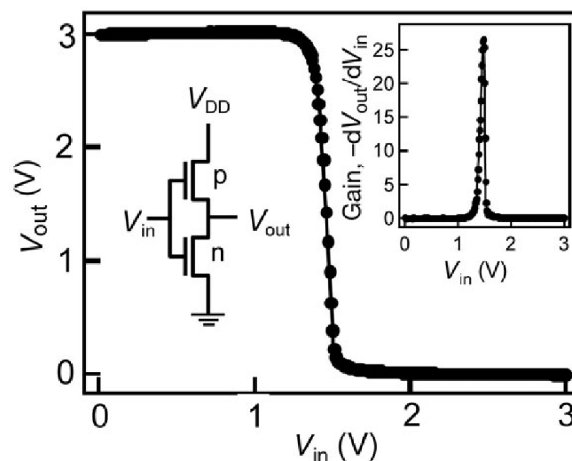
Figure 15   CdS nanobelts have been used as TFT channel materials. In conjunction with CdS
nanowires, the output-input voltage curve shows the usefulness of nanobelts in
electronic devices (from [90], with permission)

Thus far, four of the II-VI semiconductors have been successfully synthesised into a belt-like morphology. The principles that governed the devices illustrated above can be equivalently applied to all of the 1D II-VI nanostructures. The faceted surfaces of the nanobelts give advantages over other 1D nanostructures. For the case of waveguides, the facets act as reflective mirrors, trapping light in all three directions not just in the axial direction. By selecting particular polarised surfaces of the ionic wurtzite structure, the material can demonstrate a piezoelectric effect for use in electromechanical devices such as nanoactuators. It is obvious from the initial research already conducted on this group of materials that they show potential for significant impact in the field of nanoscience and technology. It is of the utmost importance that we continue to investigate these materials to further understand their structure-property relations and incorporate these structures into devices.

7   Summary

This paper presents a review on the synthesis, structure and growth mechanisms of the one-dimensional nanostructures of ZnS, CdSe, ZnSe, CdS and CdO. There are two typical morphologies for these compound semiconductor: nanobelts and nanosaws. Most of the nanostructures, except CdO, have wurtzite structure, although their bulks are dominated by zinc blend. This is a typical difference from bulk.

A common characteristic of wurtzite structure is the cation and anion terminated (0001) and (000$\bar{1}$) surfaces, respectively. The cation-terminated, catalytically active (0001) surface, while the anion-terminated (000$\bar{1}$) is chemically inactive, resulting in the asymmetric growth behaviour and the formation of saw teeth structure. In addition, we have also suggested that the phase transformation from wurtzite to zinc blend could be another factor in initiating the growth of the saw teeth. The applications of these nanostructures could be vast. Room temperature laser and complementary inverter have been demonstrated.

Acknowledgement

References

1 Norris, D.J., Sacra, A., Murray, C.B. and Bawendi, M.G. (1994) 'Measurement of the size dependent hole spectrum in CdSe quantum dots', *Phys. Rev. Lett.*, Vol. 72, p.2612.

2 Tolbert, S.H. and Alivisatos, A.P. (1994) 'Size dependence of a first order solid–solid phase transition: the wurtzite to rock salt transformation in CdSe nanocrystals', *Scienc*e, Vol. 265, p.373.

3 Bawendi, M.G., Kortan, A.R., Steigerwald, M.L. and Brus, L.E. (1989) 'X-ray structural characterization of larger CdSe semiconductor clusters', *J. Chem. Phys*., Vol. 91, p.7282.

4 Brus, L.E. (1984) 'Electron–electron and electron–hole interactions in small semiconductor crystallites: the size dependence of the lowest excited electronic state', *J. Chem. Phys*., Vol. 80, p.4403.

5 Alivisatos, A.P., Harris, A.L., Levinos, N.J., Steigerwald, M.L. and Brus, L.E. (1988) 'Electronic states of semiconductor clusters: homogeneous and inhomogeneous broadening of the optical spectrum', *J. Chem. Phys*., Vol. 89, p.4001.

6 Murray, C.B., Norris, D.J. and Bawendi, M.G. (1993) 'Synthesis and characterization of nearly monodisperse CdE (E = sulfur, selenium, tellurium) semiconductor nanocrystallites', *J. Am. Chem. Soc*., Vol. 115, p.8706.

7 Bawendi, M.G., Carroll, P.J., Wilson, W.L. and Brus, L.E. (1992) 'Luminescence properties of CdSe quantum crystallites: resonance between interior and surface localized states', *J. Chem. Phys*., Vol. 96, p.946.

8 Norris, D.J. and Bawendi, M.G. (1995) 'Structure in the lowest absorption feature of CdSe quantum dots', *J. Chem. Phys*., Vol. 103, p.5260.

9 Tran, P.T., Goldman, E.R., Anderson, G.P., Mauro, J.M. and Mattousi, H. (2002) 'Use of luminescent CdSe–ZnS nanocrystal bioconjugates in quantum dot-based nanosensors', *Phys. Stat. Sol. B*, Vol. 229, p.427.

10 Bruchez, M., Moronne, M., Gin, P., Weiss, S. and Alivisatos, A.P. (1998) 'Semiconductor nanocrystals as fluorescent biological labels', *Science*, Vol. 281, p.2013.

11 Kunets, V.P. (1998) 'Polarization self-action effect and absorption saturation in CdSe single crystals', *Phys. Stat. Sol. B*, Vol. 209, p.179.

12 Iijima, S. (1991) 'Helical microtubules of graphitic carbon', *Nature*, Vol. 354, p.56.

13 Frank, S., Poncharal, P., Wang, Z.L. and de Heer, W.A. (1998) 'Carbon nanotube quantum resistors', *Science*, Vol. 280, p.1744.

14 Poncharal, P., Wang, Z.L., Ugarte, D. and de Heer, W.A. (1999) 'Electrostatic deflections and electromechanical resonances of carbon nanotubes', *Science*, Vol. 283, p.1513.

15 Li, L.S. and Alivisatos, A.P. (2003) 'Semiconductor nanorod liquid crystals and their assembly on a substrate', *Adv. Mater.*, Vol. 15, p.408.

16 Qiao, Z., Xie, G., Tao, J., Nie, Z., Lin, Y. and Chen, X. (2002) 'Coordination polymer route to wurtzite ZnS and CdS nanorods', *J. Sol. Stat. Chem*., Vol. 166, p.49.

17 Limmer, S.J., Seraji, S., Wu, Y., Chou, T.P., Nguyen, C. and Cao, G.Z. (2002) 'Template-based growth of various oxide nanorods by sol-gel electrophoresis', *Adv. Funct. Mater*., Vol. 12, p.59.

18 Wang, J., Gudiksen, M.S., Duan, X., Cui, Y. and Lieber, C.M. (2001) 'Highly polarized photoluminescence and photodetection from single indium phosphide nanowires', *Science*, Vol. 293, p.1455.

19   Cui, Y. and Lieber, C. (2001) 'Functional nanoscale electronic devices assembled using silicon nanowire building blocks', *Science*, Vol. 291, p.851.

20   Xu, C., Xue, L., Yin, C. and Wang, G. (2003) 'Formation and photoluminescence properties of AlN nanowires', *Phys. Stat. Sol. A*, Vol. 198, p.329.

21   Zhang, Y., Wang, N., Gao, S., He, R., Miao, S., Liu, J., Zhu, J. and Zhang, X. (2002) 'A simple method to synthesize nanowires', *Chem. Mater.*, Vol. 14, p.3564.

22   Fang, Y.P., Xu, A.W., You, L.P., Song, R.Q., Yu, J.C., Zhang, H.X., Li, Q. and Liu, H.Q. (2003) 'Hydrothermal synthesis of rare earth (Tb, Y) hydroxide and oxide nanotubes', *Adv. Funct. Mater.*, Vol. 13, p.955.

23   Wang, J. and Li, Y. (2003) 'Rational synthesis of metal nanotubes and nanowires from lamellar structures', *Adv. Mater.*, Vol. 15, p.445.

24   Remskar, M., Skraba, Z., Stadelmann, P. and Levy, F. (2000) 'Structural stabilization of new compounds: MoS_2 and WS_2 micro- and nanotubes alloyed with gold and silver', *Adv. Mater.*, Vol. 12, p.814.

25   Pan, Z.W., Dai, Z.R. and Wang, Z.L. (2001) 'Nanobelts of semiconducting oxides', *Science*, Vol. 291, p.1947.

26   Seo, H.W., Bae, S.Y. and Park, J. (2003) 'Nitrogen-doped gallium phosphide nanobelts', *Appl. Phys. Lett.*, Vol. 82, p.3752.

27   Wu, Q., Hu, Z., Wang, X., Chen, Y. and Lu, Y. (2003) 'Synthesis and optical characterization of aluminum nitride nanobelts', *J. Phys. Chem. B*, Vol. 107, p.9726.

28   Liu, Z., Peng, S., Xie, Q., Hu, Z., Yang, Y. and Zhang, S. (2003) 'Large-scale synthesis of ultralong Bi_2S_3 nanoribbons via a solvothermal process', *Adv. Mater.*, Vol. 15, p.936.

29   Pan, X.S., Zhang, L.D., Meng, G.W., Wang, X.F., Wang, Y.W., Wang, C.Z. and Wu, G.S. (2002) 'Photoluminescence and infrared properties of α-Al_2O_3 nanowires and nanobelts', *J. Phys. Chem. B*, Vol. 106, p.11163.

30   Yang, P., Yan, H., Mao, S., Russo, R., Johnson, J., Saykally, R., Orris, N., Pham, J., He, R. and Choi, H. (2002) 'Controlled growth of ZnO nanowires and their optical properties', *Adv. Funct. Mater.*, Vol. 12, p.323.

31   Hiruma, K., Yazawa, M., Katsuyama, T., Ogawa, K., Haraguchi, K., Koguchi, M. and Kakibayshi, H. (1995) 'Growth and optical properties of nanometer-scale GaAs and InAs whiskers', *J. Appl. Phys.*, Vol. 77, p.447.

32   Chen, J., Wan, X. and Dong, J. (2003) 'Electronic properties of the metallic zigzag single-walled carbon nanotube ropes', *Phys. Stat. Sol. B*, Vol. 239, p.152.

33   Wong, E.W., Sheehan, P.E. and Lieber, C.M. (1997) 'Nanobeam mechanics: elasticity, strength, and toughness of nanorods and nanotubes', *Science*, Vol. 277, p.1971.

34   Wang, Z.L., Gao, R.P., Pan, Z.W. and Dai, Z.R. (2001) 'Nano-scale mechanics of nanotubes, nanowires, and nanobelts', *Adv. Eng. Mater.*, Vol. 3, p.657.

35   Cui, Y., Wei, Q., Park, H. and Lieber, C.M. (2001) 'Nanowire nanosensors for highly sensitive and selective detection of biological and chemical species', *Science*, Vol. 293, p.1289.

36   Kim, P. and Lieber, C.M. (1999) 'Nanotube nanotweezers', *Science*, Vol. 286, p.2148.

37   Yan, H., Johnson, J., Law, M., He, R., Knutsen, K., McKinney, J.R., Pham, J., Saykally, R. and Yang, P. (2003) 'ZnO nanoribbon microcavity lasers', *Adv. Mater.*, Vol. 15, p.1907.

38   Wang, Z.L. (2004) 'Nanostructures of ZnO', *Materials Today*, Vol. 7, No. 6, p.26.

39   Lefebvre, P., Richard, T., Allegre, J. and Mathieu, H. (1996) 'Measurement of the optical band gap and crystal-field splitting in wurtzite CdTe', *Phys. Rev. B*, Vol. 53, p.15440.

40   Wang, Y., Zhang, L., Liang, C., Wang, G. and Peng, X. (2002) 'Catalytic growth and photoluminescence properties of semiconductor single-crystal ZnS nanowires', *Chem. Phys. Lett.*, Vol. 357, p.314.

41 Jiang, Y., Meng, X., Yiu, W., Liu, J., Ding, J., Lee, C. and Lee, S. (2004) 'Zinc selenide nanoribbons and nanowires', *J. Phys. Chem. B*, Vol. 108, p.2784.

42 Hughes, W.L. and Wang, Z.L. (2003) 'Nanobelts as nanocantilevers', *Appl. Phys. Lett*., Vol. 82, p.2886.

43 Chen, G.Y., Thundat, T., Wachter, E.A. and Warmack, R.A. (1995) 'Adsorption-induced surface stress and its effects on resonance frequency of microcantilevers', *J. Appl. Phys*., Vol. 77, p.3618.

44 Fritz, J., Baller, M.K., Lang, H.P., Rothuizen, H., Vettiger, P., Meyer, E., Guntherodt, H.J., Gerber, C. and Gimzewski, J.K. (2000) 'Translating biomolecular recognition into nanomechanics', *Science*, Vol. 288, p.316.

45 Wu, G., Ji, H., Hansen, K., Thundat, T., Datar, R., Cote, R., Hagan, M.F., Chakraborty, A.K. and Majumdar, A. (2001) *PNAS*, Vol. 98, p.1560.

46 Dai, Z.R., Pan, Z.W. and Wang, Z.L. (2003) 'Novel nanostructures of functional oxides synthesised by thermal evapouration', *Adv. Funct. Mater.*, Vol. 13, p.9.

47 Ma, C., Moore, D., Li, J. and Wang, Z.L. (2003) 'Nanobelts, nanocombs, and nanowindmills of wurtzite ZnS', *Adv. Mater*., Vol. 15, p.228.

48 Jiang, Y., Meng, X., Liu, J., Xie, Z., Lee, C. and Lee, S. (2003) 'Hydrogen-assisted thermal evapouration synthesis of ZnS nanoribbons on a large scale', *Adv. Mater.*, Vol. 15, p.323.

49 Zhu, Y., Bando, Y. and Xue, D. (2003) 'Spontaneous growth and luminescence of zinc sulfide nanobelts', *Appl. Phys. Lett*., Vol. 82, p.1769.

50 Li, Q. and Wang, C. (2003) 'Fabrication of wurtzite ZnS nanobelts via simple thermal evapouration', *Appl. Phys. Lett*., Vol. 83, p.359.

51 Hu, P., Liu, Y., Fu, L., Cao, L. and Zhu, D. (2004) 'Self-assembled growth of ZnS nanobelt networks', *J. Phys. Chem. B*., Vol. 108, p.936.

52 Li, Y., You, L., Duan, R., Shi, P., Du, H., Qiao, Y. and Qin, G. (2004) 'Straight ZnS nanobelts with wurtzite structure synthesised by the vapour phase transport process and their crystallization and photoluminescence properties', *Nanotechnolg*y, Vol. 15, p.581.

53 Moore, D., Roning, C., Ma, C. and Wang, Z.L. (2004) 'Wurtzite ZnS nanosaws produced by polar surfaces', *Chem. Phys. Lett.*, Vol. 385, p.8.

54 Huynh, W.U., Peng, X. and Alivisatos, A.P. (1999) 'CdSe nanocrystal rods/ poly(3-hexylthiophene) composite photovoltaic devices', *Adv. Mater*., Vol. 11, p.923.

55 Wang, W., Geng, Y., Yan, P., Liu, F., Xie, Y. and Qian, Y. (1999) 'Synthesis and characterization of MSe (M = Zn, Cd) nanorods by a new solvothermal method', *Inorg. Chem. Comm*, Vol. 2, p.83.

56 Artemyev, M., Moller, B. and Woggon, U. (2003) 'Unidirectional alignment of CdSe nanorods', *Nano Lett*., Vol. 3, p.509.

57 Hu, J., Li, L., Yang, W., Manna, L., Ang, L. and Alivisatos, A.P. (2001) 'Linearly polarized emission from colloidal semiconductor quantum rods', *Science*, Vol. 292, p.2060.

58 Peng, X.G., Manna, L., Yang, W.D., Wickman, J., Scher, E., Kadavanich, A. and Alivisatos, A.P. (2004) 'Shape control of CdSe nanocrystals', *Nature*, Vol. 404, p.59.

59 Peng, X.S., Zhang, J., Wang, X.F., Wang, Y.W., Zhao, L.X., Meng, G.W. and Zhang, L.D. (2001) 'Synthesis of highly ordered CdSe nanowire arrays embedded in anodic alumina membrane by electrodeposition in ammonia alkaline solution', *Chem. Phys. Lett*., Vol. 343, p.470.

60 Xu, D.S., Shi, X.S., Guo, G.L., Gui, L.L. and Tang, Y.Q. (2000) 'Electrochemical preparation of CdSe nanowire arrays', *J. Phys. Chem. B*, Vol. 104, p.5061.

61 Jiang, X.C., Mayers, B., Herricks, T. and Xia, Y.N. (2003) 'Direct synthesis of Se@CdSe nanocables and CdSe nanotubes by reacting cadmium salts with Se nanowires', *Adv. Mater*., Vol. 15, p.1740.

62   Wu, Y.W., Wu, C.S., Chen, C.C. and Chen, C.D. (2003) 'Fabrication of two-dimensional arrays of CdSe pillars using e-beam lithography and electrochemical deposition', *Adv. Mater.*, Vol. 15, p.49.

63   Ma, C., Ding, Y., Moore, D., Wang, X. and Wang, Z.L. (2004) 'Singel-crystal CdSe nanosaws', *J. Am. Chem. Soc.*, Vol. 126, p.708.

64   Ding, Y., Ma, C., Wang, X.D. and Wang, Z.L. (2004) 'Formation process of gold catalyzed wurtzite nanostructures', *Adv. Mater.*, in press.

65   Wang, Z.L., Kong, X.Y. and Zuo, J.M. (2003) 'Self-catalyzing and phase transformation in the formation of CdSe nanosaws', *Adv. Mater.,* Vol. 16, p.1740.

66   Dong, L., Jiao, J., Coulter, M. and Love, L. (2003) 'Catalytic growth of CdS nanobelts and nanowires on tungsten substrates', *Chem. Phys. Lett.*, Vol. 376, p.653.

67   Liu, W., Jia, C., Yao, L., Cai, W. and Li, X. (2004) 'CdS nanobelts on Si substrates', *Chem. Lett.*, Vol. 33, p.228.

68   Vigue, F., Vennegues, P., Vezian, S., Laugt, M. and Faurie, J-P. (2001) 'Defect characterization in ZnO layers grown by plasma-enhanced molecular-beam epitaxy on (0001) sapphire substrates', *Appl. Phys. Lett.*, Vol. 79, p.194.

69   Spence, J.C.H. and Zuo, J.M. (1992) *Electron Microdiffraction*, Plenum, New York, NY.

70   Yeh, C.Y., Lu, Z.W., Froyen, S. and Zunger, A. (1992) 'Zinc-blende–wurtzite polytypism in semiconductors', *Phys. Rev. B*, Vol. 46, p.10086.

71   Gutowski, J., Michler, P., Ruckmann, H.I., Brunig, H.G., Rowe, M., Sebald, K. and Voss, T. (2002) 'Excitons in wide-gap semiconductors: coherence, dynamics, and lasing', *Phys. Stat, Sol. B*, Vol. 234, p.70.

72   Pawaskar, N.R., Sathaye, S.D., Bhadhade, M.M. and Patil, K.R. (2002) 'Applicability of liquid–liquid interface reaction technique for the preparation of zinc sulfide nano particulate thin films', *Mater. Res. Bull.*, Vol. 37, p.1539.

73   Jiang, X., Xie, Y., Lu, J., Zhu, L., He, W. and Qian, Y. (2001) 'Simultaneous in situ formation of ZnS nanowires in a liquid crystal template by γ-irradiation', *Chem. Mater.*, Vol. 13, p.1213.

74   Elidrissi, B., Addou, M., Regragui, M., Bougrine, A., Kachoune, A. and Bernecde, J.C. (2001) 'Structure, composition and optical properties of ZnS thin films prepared by spray pyrolysis', *Mater. Chem. Phys.*, Vol. 68, p.175.

75   Yamaga, S., Yoshikawa, A. and Kasai, H. (1998) *J. Cryst. Growth*, Vol. 86, p.252.

76   Falcony, C., Garcia, M., Ortiz, A. and Alonso, J.C. (1992) 'Luminescent properties of ZnS:Mn films deposited by spray pyrolysis', *J. Appl. Phys.*, Vol. 72, p.1525.

77   Prevenslik, T.V. (2000) 'Acoustoluminescence and sonoluminescence', *J. Lumin.*, Vol. 87–89, p.1210.

78   Xu, C.N., Watanabe, T., Akiyama, M. and Zheng, X.G. (1999) 'Preparation and characteristics of highly triboluminescent ZnS film', *Mater. Res. Bull.*, Vol. 34, p.1491.

79   Tang, W. and Cameron, D.C. (1996) 'Electroluminescent zinc sulphide devices produced by sol-gel processing', *Thin Solid Films*, Vol. 280, p.221.

80   Chen, W., Wang, Z., Lin, Z. and Lin, L. (1995) 'Thermoluminescence of ZnS nanoparticles', *Appl. Phys. Lett.*, Vol. 70, p.1465.

81   Rakhshani, A.E. (1997) 'Electrodeposited CdTe – optical properties', *J. Appl. Phys.*, Vol. 81, p.7988.

82   Lischka, K. (1997) 'Epitaxial ZnSe and cubic GaN: wide-band-gap semiconductors with similar properties?', *Phys. Stat. Sol. B*, Vol. 202, p.673.

83   Basol, B.M. (1988) *Sol. Cells*, Vol. 23, p.69.

84   Ando, K., Ishikura, H., Fukunaga, Y., Kubota, T., Maeta, H., Abe, T. and Kasada, H. (2002) 'Highly efficient blue-ultraviolet photodetectors based on II-VI wide-bandgap compound semiconductors', *Phys. Stat. Sol. B*, Vol. 229, p.1065.

85 Duan, X., Huang, Y., Agarwal, R. and Lieber, C.M. (2003) 'Single-nanowire electrically driven lasers', *Nature*, Vol. 421, p.241.

86 Covin, V.L., Schlamp, M.C. and Alivisatos, A.P. (1994) 'Light emitting diodes made from cadmium selenide nanocrystals and a semiconducting polymer', *Nature*, Vol. 370, p.354.

87 Chan, W.C. and Nie, S.M. (1998) 'Quantum dot bioconjugates for ultrasensitive nonisotopic detection', *Science*, Vol. 281, p.2016.

88 Zapien, J.A., Jiang, Y., Meng, X.M., Chen, W., Au, F.C.K., Lifshitz, Y. and Lee, S.T. (2004) 'Room-temperature single nanoribbon lasers', *Appl. Phys. Lett.*, Vol. 84, p.1189.

89 Huang, M.H., Mao, S., Feick, H., Yan, H., Wu, Y., Kind, H., Webber, E., Russo, R. and Yang, P. (2001) 'Room-temperature ultraviolet nanowire nanolasers', *Science*, Vol. 292, p.1897.

90 Duan, X., Niu, C., Sahi, V., Chen, J., Parce, J.W., Empedolce, S. and Goldman, J.L. (2003) 'High-performance thin-film transistors using semiconductor nanowires and nanoribbons', *Nature*, Vol. 425, p.274.